HST Imaging of the Circumstellar Nebulosity of T Tauri

Karl R. Stapelfeldt[1], Christopher J. Burrows[2,3], John E. Krist[2], Alan M. Watson[4], Gilda E. Ballester[5], John T. Clarke[5], David Crisp[1], Robin W. Evans[1], John S. Gallagher III[6], Richard E. Griffiths[7], J. Jeff Hester[8], John G. Hoessel[6], Jon A. Holtzman[9], Jeremy R. Mould[10], Paul A. Scowen[8], John T. Trauger[1], and James A. Westphal[11]

Subject headings: circumstellar matter — stars: individual (T Tau) – stars: pre-main sequence

Received _____; accepted _____

---

[1]MS 183-900 Jet Propulsion Laboratory, 4800 Oak Grove Drive Pasadena CA 91109

[2]Space Telescope Science Institute, Baltimore, MD 21218

[3]Astrophysics Division, Space Science Department, European Space Agency

[4]Instituto de Astronomi'a UNAM, 58090 Morelia, Michoacan, Mexico

[5]Dept. of Atmospheric, Oceanic, and Space Sciences, University of Michigan, 2455 Hayward, Ann Arbor MI 48109

[6]Dept. of Astronomy, University of Wisconsin, 475 N. Charter St., Madison WI 53706

[7]Dept. of Physics, Carnegie-Mellon University, Wean Hall, 5000 Forbes Ave., Pittsburgh PA 15213

[8]Dept. of Physics and Astronomy, Arizona State University, Tyler Mall, Tempe AZ 85287

[9]Dept. of Astronomy, New Mexico State University, Box 30001, Dept. 4500, Las Cruces NM 88003

[10]Mt. Stromlo and Siding Springs Observatories, Australian National University, Weston Creek Post Office, ACT 2611 Australia

[11]Division of Geological and Planetary Sciences, MS 170-25 Caltech, Pasadena CA 91125

Submitted to the Astrophysical Journal

ABSTRACT

Short exposure Planetary Camera images of T Tauri have been obtained using broadband filters spanning the wavelength range 0.55-0.80 μm. The optically visible star lies very close to an arc of reflection nebulosity. The arc's northern arm extends approximately 5″ from the star, while its southwestern arm appears brighter and extends only 2″. The arc shows an approximate symmetry along an axis toward the WNW, the direction of Hind's Nebula and the blueshifted molecular outflow. The morphology of the reflected light is similar to models of scattered light within an illuminated, axisymmetric outflow cavity in a circumbinary envelope, viewed $\approx$ 45°from the outflow axis. However, our model images do not successfully account for the amount of limb brightening which is seen. No optical counterpart to the infrared companion is seen to a limiting magnitude of V=19.6, which suggests $A_V > 7$ mag toward this source. There is no evidence for an optical tertiary, to a limiting ΔV=5.1 mag fainter than the primary, at the position where such an object has been previously reported.

1. Introduction

T Tauri (HBC 35) has long been considered a prototype pre-main sequence star (Joy 1945), but is now known to be a very unique system. The variable, optically visible star is one component of a close binary, with a cool infrared companion 0.7″ to the S (Dyck, Simon, and Zuckerman 1982). The companion, known as T Tau S, has not yet been detected at optical wavelengths even though it produces the greater part of the bolometric luminosity of the system (Ghez *et al.* 1991). A third star was reported 0.″27 N of the primary (Nisenson *et al.* 1985), apparently confirmed in the infrared (Maihara and Kataza 1991), but not subsequently seen (Gorham 1992). In addition, two nebulae are associated with T Tau. Burnham's Nebula (HH 255) is an extended structure of reflection and emission centered on the binary and extending as far as 10″. A separate variable reflection nebula, NGC 1555 (Hind's Nebula), is located 30″ to the west.

Evidence for circumstellar material in the T Tau system is provided by far-infrared and millimeter continuum emission. IRAS detected the source as PSC 04190+1924. The spectral energy distribution has been modeled with warm circumstellar dust distributed in both a circumprimary disk (Adams, Lada, and Shu 1987) and a more extended circumstellar envelope (Calvet *et al.* 1994). Recent millimeter interferometry appears to confirm the presence of a circumstellar disk around the optically visible star T Tau N (Akeson *et al.* 1998; Hogerheijde *et al.* 1997), with a diameter of less than 100 AU and mass near 10^{-2} $M_{\odot}$. Although no millimeter continuum is detected about the companion, mid-infrared excesses clearly indicate the presence of circumstellar material there as well (Herbst, Robberto, and Beckwith 1997).

The kinematics of the region surrounding T Tau have been found to be very complex. High velocity CO emission from the system has been mapped by Schuster, Harris, and Russell 1997 and Levreault 1988, and shows a preponderance of blueshifted emission west

of the binary. Near-infrared molecular hydrogen emission is widely distributed throughout Burnham's Nebula in knots and filaments (Herbst *et al.* 1996,van Langevelde *et al.* 1994). Optical spectroscopy has provided the most detailed information, with as many as five distinct kinematic components present in the emission line spectra (Böhm and Solf 1994). These suggest that both the primary and companion drive separate bipolar outflows. The giant Herbig-Haro flow recently discovered to the N and S of the system is believed to trace the outflow from the infrared companion (Reipurth, Bally, and Devine 1997).

Ground based coronagraphic images (Nakajima and Golimowski 1995, Robberto *et al.* 1995) have revealed the structure of Burnham's Nebula outside a radius of 2″ (300 AU). In hopes of detecting the companion star directly in the optical, and resolving the circumstellar nebulosity to clarify the distribution of material with 2″ of the binary, we have observed T Tauri with the Hubble Space Telescope. We report on the observations and results in sections II. and III., and then develop a scattered light model for the reflection nebulosity in section IV.

2. Observations

Three images of T Tau were obtained on 1994 March 4 using the Wide Field and Planetary Camera 2 (WFPC2, Burrows 1995) aboard the Hubble Space Telescope (HST). The star was imaged in the F/28.3 Planetary Camera (PC), in which the 0.″05 full width half maximum point spread function (PSF) of HST at λ= 555 nm is sampled at 0.″046 per pixel. The filters and exposure times were F555W, 14 sec; F675W, 5 sec; and F814W, 3 sec. These filters are analogues of the Johnson V, R, and I passbands respectively. A gain setting of 14 electrons per DN was used to maximize the dynamic range in the data. Image processing steps included subtraction of bias levels derived from rows 8-14 of the overscan, subtraction of a superbias image, subtraction of a composite dark frame scaled to the

individual exposure times, the removal of cosmic rays via replacement of affected pixels by a local median, and flat fielding. We adopt the photometric calibration of Holtzman *et al.* 1995. Most regions of the image are read noise limited. In these areas, the short exposure times and small pixel size combine to produce 3σ limiting surface brightnesses of only 17.8, 16.3, and 15.3 mag arcsec^{-2} in the F555W, F675W and F814W images respectively. Close to the star, the limiting surface brightness magnitude is lower because of the difficulty of exactly subtracting the stellar PSF.

3. Results

The F555W reduced image of T Tau is shown in Fig. 1, panel a. The images are saturated within 0.″1 of the star in all three filters, which has resulted in some bleeding of excess charge up and down the CCD columns (left and right as seen in the figure). The stellar image includes prominent diffraction spikes at 45°angles, and the PSF skirt which fades with distance from the stellar position. A faint near-focus point source image is present 0.″9 NE of the star superposed on circumstellar nebulosity. The location and brightness of this feature are consistent with an expected ghost image originating when light from T Tau is reflected from the primary image on the CCD and returned to the CCD by an additional reflection from the curved CCD field flattener. In the WFPC2 cameras, these ghosts appear offset from the saturated star along a direction oriented away from the field center.

There are two features which are not part of the PSF structure and which appear in all three passbands. These are filaments of nebulosity which extend to the upper right and lower right (N and SW) in Fig. 1 panel a.

The circumstellar nebular structure can be seen more clearly when a reference PSF is subtracted from the images. Two approaches were tried; the relative merits of each are

discussed further by Krist *et al.* 1997. The first used idealized theoretical PSFs (TinyTim; Krist 1995) calculated for these filters at the field position of T Tau in the science images. This approach did not produce the best result because the model does not include known scattering effects at the CCD detector. The second approach was to use saturated WFPC2 stellar images taken in the same filters for reference PSFs. Images of the weak line T Tauri star SAO 76411A, which was found to lack any circumstellar nebulosity, were used. These subtraction results are somewhat better, and are shown in Fig. 1, panels b-d for each of the three filters. In both cases, the alignment and normalization of the reference PSF was accomplished by minimizing the brightness of the symmetric PSF skirt in the difference images. Saturated pixels in both the target and reference PSF images were given zero weight during optimization of the subtraction. Neither the theoretical nor the observed PSFs allow a perfect subtraction free of artifacts; the best difference images still show low-level residual diffraction spikes which confuse the view of the circumstellar features at PAs 80, 170, 260, and 350 degrees. In addition, saturation column bleeding in the images of T Tau and the observed PSF star obscures the region closest to the star at position angles 125 and 305 degrees. Affected pixels lie within the dark horizontal band in Fig. 1 panels b-d.

The subtracted images show that the nebulosity has the form of a continuous, roughly parabolic arc that is concave open to the WNW and has a thickness of $0\farcs5$ to $1\farcs0$. A contour map of the F555W surface brightness is shown in Fig. 2. The arc is more closely centered on the primary star than on the infrared companion. T Tauri N is positioned near the inside edge of the arc, and offset by about $0\farcs3$. The arc is brightest immediately adjacent to the primary, and falls rapidly in surface brightness until lost in the read noise at the limiting surface brightnesses quoted above. T Tau S lies just outside of the arc, displaced from the arc's center of symmetry and region of maximum brightness. The arc is not symmetrical about the optically visible star. The nebulosity is significantly brighter on the SW side of

the star compared to the NW side at the same distance. Conversely, the NW arm of the arc is much longer than that to the SW, is somewhat wider, and is more curved. The NW arm extends 5″ from the star in F555W but only about 4″ in the other two filters because their limiting magnitude is lower. The SW arm is only 2.″8 long, has more sharply defined edges, and has the same length in all three passbands. This suggests that edges of the SW arm are defined by the intrinsic source structure, and not by the sensitivity level in the images. Note the small "island" of nebulosity present within the nebular arc, approximately 1.3″ NNW of T Tau N. This is a real source feature well-separated from the diffraction spike residuals. It is appears in the F555W image but not at F675W and F814W; this is most likley due to the lower sensitivity of the latter images.

No major color differences are seen within the nebular arc between the three wavelengths which were observed. The brightest Herbig-Haro emission lines in Burnham's Nebula are Hα, [S II], and [O I] (Solf, Böhm, and Raga 1988), all of which fall in the bandpass of the F675W filter. If these lines contributed significantly to the nebular morphology seen by HST, they would produce clear morphological differences between the F675W and F814W images. The lack of features unique to the F675W filter strongly argues that the arc is primarily reflection nebulosity in all three bandpasses. A careful comparison of the F555W and F814W images reveals that the inner edge of the NW arm is bluer than the arm a whole, while its outer edge may be redder. It is hard to quantify these gradients because they occur where the signal levels are only a few DN. There is no evidence for any color gradient in the SW arm. Longer exposures are needed to confirm the color gradients in the NW arm, and to detect any of the Herbig-Haro emission knots known to be associated with the system.

The nebula seen in the HST images appears to be the inner portion of a larger arc seen in the ground based measurements of Nakajima and Golimowski 1995 and Robberto *et al.* 1995. The latter observations extend to much fainter levels (about 22 mag arcsec^{-2}), but

provide no data beneath the 2″ radii occulting masks used, and have an order of magnitude less spatial resolution. Both groups show that the NW arm continues to gently curve outward in the same direction, to grow in width and to fade in surface brightness away from the star. They also agree that at low surface brightness levels the SW arm appears to abruptly change direction from the SW course that we observe to SE. This behavior is not seen in the HST images because the brightness of the SE extension lies below the sensitivity level of our observations (V= 17.8 mag arcsec^{-2}).

Photometric measurements of T Tau N are required to quantify the relative brightness of circumstellar features in comparison to the direct starlight. The star is saturated in all the HST images, but useful photometry can still be obtained using the calibration of the WFPC2 CCD well depths given by Gilliland 1994. The total number of detected photoelectrons is a sum of the counts outside the saturation region and the number of saturated pixels multiplied by the well depth. A 128 pixel (5.8″) square aperture was used to include all of the brightest nebulosity. We obtain integrated magnitudes (star + nebula) of 10.06, 9.40, and 8.82 in the F555W, F675W, and F814W bandpasses. We estimate the systematic errors at ± 0.05 mag. We find that the total integrated brightness of the reflection nebulosity is about 20% of the direct starlight from T Tau N in all three colors. The F555W magnitude of the system is in reasonable agreement with published groundbased V magnitudes; however, the F555W-F675W and F555W-F814W colors are about 0.1 and 0.3 mag bluer than the the corresponding groundbased V-R and V-I colors (Kenyon and Hartmann 1995; Strom *et al.* 1989). Color corrections to the WFPC2 photometric system are not large enough to resolve this discrepancy (Holtzman *et al.* 1995), and thus an intrinsic variation in source color is indicated.

To establish limiting magnitudes for companion stars, Planetary Camera point spread functions of various amplitudes were added into the images at the positions of T Tau S and the supposed optical tertiary. For each image a scaling level for the PSF was determined,

below which the PSF became indistinguishable by eye against the local background noise. For the infrared companion, this leads to the following WFPC2 limiting magnitudes: V>19.6; R>18.2; and I>17.4. For the supposed optical tertiary, our limiting magnitude is only V> 15.3 because of the greater noise from the PSF wings very close to T Tau N.

4. Discussion

4.1. Constraints on Companion Stars

No optical counterpart to T Tau S is seen in these images to a limiting magnitude V> 19.6, and thus this object is at least 9.5 magnitudes fainter than T Tau N at this wavelength. Unfortunately this observation only weakly constrains the visual extinction toward the infrared companion. A simple blackbody stellar photosphere corresponding to the post-outburst K magnitude and minimum luminosity of T Tau S (6.5 mag and 15 $L_{\odot}$; Ghez *et al.* 1991) would have a V=9.6. The actual spectral energy distribution is certainly more complex, with veiling emission and thermal dust continuum contributing significant excesses above the stellar photosphere. Thus it is difficult to say with certainty what intrinsic V magnitude should be expected for this source. A limiting case that allows the faintest possible intrinsic V magnitude would be a very cool stellar photosphere ($\log T_{eff} = 3.5$) combined with a large veiling factor of 4 at $\lambda = 2.2$ μm. Using the observed K magnitude, these assumptions would imply a photospheric V=12.5 and luminosity of 2 $L_{\odot}$. Thus we suggest the visual extinction toward T Tau S is at least 7 magnitudes. This limit lies at the upper edge of the extinction range ($4 < A_V < 7$) estimated by Ghez *et al.* 1991 from the strength of the silicate absorption.

There is no evidence in our images for the optical tertiary star reported by Nisenson *et al.* 1985 and Maihara and Kataza 1991. At the position reported for this source our images

are dominated by PSF artifacts from the bright primary, and thus our limiting magnitude is only ΔV=5.2. Nevertheless, this object would have been detected if it had maintained the same brightness and position which had been first reported. Our observations reaffirm the conclusions of Gorham 1992 that this object must have faded by nearly a magnitude since 1984 if the earlier detections are to be considered valid.

4.2. Nebula Morphology and the Geometry of the T Tau System

The major nebular feature near the T Tau binary is the arc of reflection nebulosity which appears to be centered on, and illuminated by, the primary star. The images of Nakajima and Golimowski 1995 show that the N arm of the arc extends to the NW to a radial distance of about 10″, about twice the length seen in these short HST exposures. Neither arm of the arc appears to coincide with the locations of high velocity gas as traced by optical spectroscopy (Böhm and Solf 1994) or shocked molecular hydrogen emission (Herbst, Robberto, and Beckwith 1997). It therefore appears to be a distinct structure which traces the boundary of dense material in the circumbinary region.

It is difficult to assess what role, if any, the companion star plays in defining the distribution of scattered light that is seen. Residual diffraction spikes pass close to the position of the companion, precluding detection of any faint nebulosity there. The companion presumably lies behind the circumbinary material which is responsible for both its extinction and the nearby scattered visible light from T Tau N. The arc appears brighter and more truncated near the projected position of T Tau S. It is tempting to speculate that the companion might be responsible for this, perhaps due to effects of its outflow or gravity on the distribution of scattering material. Alternatively, light from T Tau S might play some role in illuminating this part of the nebula. From our data, there is no clear way to distinguish among these possibilities.

The standard paradigm for the environment around an isolated protostar is a centrifugally supported accretion disk surrounded by a more tenuous infalling envelope that extends to much higher latitudes, and with bipolar cavities in the envelope cleared by the action of jets and winds from the inner disk and protostar. This paradigm must be significantly modified for the case of T Tau because we know that two stars have formed at a separation of at least 100 AU. Presumably both stars share a common infalling envelope, the residual material of the molecular cloud core from which they formed. There is evidence to suggest that both stars drive collimated outflows which produce shocked line emission (Böhm and Solf 1994) and which may carve cavities in their common envelope. Each star may have an associated accretion disk with a tidally truncated outer radius perhaps 1/4 the physical separation of the pair. They may share an outer circumbinary disk, tidally truncated at an inner radius of perhaps 4 times the binary separation. Such disk structures could survive for many dynamical timescales.

Given all of these expected features in the circumbinary environment, which is most likely to be related to the nebular arc seen about T Tau N? A natural possibility to investigate is an outflow cavity blown by winds or jets from T Tau N into the extended envelope needed to explain the IRAS 100 μm flux. Such a cavity would be seen via scattered light from T Tau N, and could appear limb brightened. The approximate symmetry axis of the nebular arc is toward the WNW, requiring that the cavity and corresponding outflow be aligned near PA 300°. An outflow from the primary at this PA is consistent with the blueshifted optical emission lines and CO outflow to the west of T Tau. The SE extension to the scattered light seen by Nakajima and Golimowski 1995 could be interpreted as part of the counter-cavity associated with the redshifted lobe of a bipolar outflow from T Tau N. If our scenario is correct, the circumstellar disk of T Tau N should eventually be resolved along PA 30°, perpendicular to the axis of the proposed outflow cavity. The separate outflow from the companion would be obscured from view in our scenario. This outflow is

now known to extend N-S (Reipurth, Bally, and Devine 1997), and thus probably includes the bright near-infrared H_2 emission knot found by Herbst *et al.* 1996.

Predicted scattered light images for outflow cavities appear in the literature (Whitney and Hartmann 1993), but are presented at low spatial resolutions not well-suited for comparison with HST images. To test the applicability of such models to the HST images of T Tau, we calculated our own simple axisymmetric models for the reflected light produced when a circumstellar envelope with a cavity is illuminated by a central star. The brightness contribution of each volume element in the circumstellar density distribution is weighted according to its optical depth, extinction toward the star and toward the observer, the inverse-square law, and a Henyey-Greenstein scattering phase function. Dust properties appropriate to λ =0.5 μm were adopted: opacity of 250 cm^2 gm^{-1}, albedo of 0.5, and asymmetry parameter $g = 0.44$. In applying such models to the T Tau images, we ignore the obvious nebular asymmetries which the axisymmetric model cannot account for. Instead we seek only to determine if a cavity model can simultaneously reproduce the nebular arc's overall curvature, thickness, limb brightening, and location with respect to the illuminating star.

Following Whitney and Hartmann 1993, we adopt the density distribution of Ulrich 1976, appropriate to a collapsing envelope with rotation

$$\rho = \frac{\dot{M}}{4\pi}(GMR_c^3)^{-1/2}\left(\frac{R_c}{R}\right)^{3/2}\left(1+\frac{\sin\theta}{\sin\theta_0}\right)^{-1/2}\left(\frac{\sin\theta}{\sin\theta_0}+\frac{2\sin^2\theta_0 R_c}{R}\right)^{-1} \qquad (1)$$

where $\dot{M}$ is the mass infall rate, M is the mass of the central object, R_c is the centrifugal radius, R and θ are the spherical coordinate radius and latitude, and θ_0 defines the direction of the initial streamline of the infalling material. This density law is an oversimplification since it takes no account of the binarity of the central object, but it should be an adequate description of the density near the cavity boundary. A functional form z= ar^β was chosen

for the cavity geometry in cylindrical coordinates. The bipolar cavities are considered to be completely evacuated ($\rho = 0$ for $|z| > ar^{\beta}$), whereas elsewhere the density is given by (1). We initially chose $r_c = 100$ AU, $\dot{M} = 3\text{x}10^{-6}$ $M_{\odot}$ yr^{-1}, and M= 2.0 $M_{\odot}$ (Calvet *et al.* 1994). This leaves the three geometrical parameters (a, β, θ) to determine from the images.

The images should be able to constrain the range of possible parameters for the model cavity geometry. If we assume that the nebular arc corresponds to the projected cavity wall, then the small offset distance between the star and the arc of reflected light requires that we view the system nearly along the edge of the cavity wall. This can be quantified in terms of the "impact parameter" b, the observed offset between the star and the projected edge of the cavity. Geometrically b is defined with respect to the locatation where the cavity's curvature brings it tangent to the observer's line of sight. The cylindrical coordinate radius at the tangent point is related to b by $r = b\beta/(\beta - 1)\sin\theta$; see Fig. 3. Substituting this relation into $dz/dr = \tan\theta$, the cavity shape parameter a can be solved for in terms of θ, β, and b:

$$a = \frac{\tan\theta}{\beta}\left[\frac{(\beta - 1)\sin\theta}{b\beta}\right]^{(\beta-1)} \tag{2}$$

The value of b can be measured from the T Tau images, and is about 7 pixels (45 AU). In addition to reproducing the observed impact parameter, the model cavity must reproduce the size and shape of the arc itself. This is effectively a second constraint on the three parameters, as can be seen by inspection for the case of θ near zero: the "span" of the model arc should match that of the observed nebula at a fiducial distance. By combining these two requirements, an optimized solution for the cavity geometry (a, β) can be found for any specified observer latitude θ.

Model reflection nebulae were calculated over a range of observer latitudes and their corresponding cavity shapes. Some parameter space exploration was performed manually,

yielding the "optimal" result shown along with the F555W image in Fig. 4. The preferred orientation of the symmetry axis is along PA 300°. We found that envelope density normalizations less than $\dot{M} = 10^{-6}$ caused the cavity wall to become partially transparent beyond a radius of a few hundred AU. Such cases produce diffuse model nebulae which are an unsatisfactory match to the T Tau nebular arc. When viewed from low latitudes ($\theta = 25°$; Fig. 4a), we found that the intrinsic curvature of the cavity must be large ($\beta > 3$) in order to reproduce the shape of the arc about T Tau N. However, this model also predicts a large envelope extinction toward the star ($A_V = 9$ mag) and a visible counter-nebula on the opposite side of the star from the main cavity. Since neither of these is observed, low latitude models appear to be ruled out. From higher latitudes ($\theta = 65°$; Fig. 4c), the model images become insensitive to β because the cavity's cylindrical cross-section becomes the dominant contributor to its observed curvature. At the nearly pole-on aspect suggested by the inclination of the stellar rotation axis (Herbst *et al.* 1986), none of our cavity models produce a nebular arc like that seen in the HST images. In this case ($\theta = 85°$) the models lack extended arms of reflected light, show too much circular symmetry, and formally have zero extinction toward the star. The best match to the HST image is obtained by our models at latitude of $45° - 65°$, where the nebula arms are prominent, the counter-nebula is not seen, and the predicted $A_V = 3.0$ mag is close to the observed value of 2 mag.

The kinematics of the shocked optical emission lines lend support to our conclusion that the outflow cavity of T Tau N is viewed from mid-latitudes. Böhm and Solf 1994 report a shocked emission knot 3″ west of T Tau N, within the bounds of the proposed cavity, and with a radial velocity of -120 km s^{-1}. If this knot originates in a Herbig-Haro jet with typical flow speeds of 200 km s^{-1}, then its radial velocity would imply that the outflow and its aligned cavity are observed at a latitude of only 30° (the outflow is 30° from the plane of the sky). Such a jet-derived inclination seems very relevant given a jet's probable role in defining the cavity's geometry. Although our cavity models do not accommodate an

inclination as low as 30°, the jet radial velocity measurements clearly favor lower latitude observing aspects than suggested by the orientation of the stellar rotation axis. Schuster, Harris, and Russell 1997 derive a similar inclination based on an analysis of the kinematics of the CO outflow and its relationship to NGC 1555.

Our illuminated cavity models for the T Tau nebular arc suffer from two general problems not related to any preferred orientation. First, they predict a relatively narrow limb-brightened edge for the cavity (of order the telescope resolution, or pixel size) compared to what is actually seen. Convolution of the models with the telescope PSF falls well short of resolving this difficulty. Secondly, the limb-to-interior contrast of the model cavities is always less than 2. The observed contrast is greater than 4. One might think that the limb brightening could be increased by adopting a density distribution that included a swept-up shell, effectively increasing the local density of scatters at the cavity wall. However, such a model also increases the interior brightness of the cavity, and leaves the limb-to-interior contrast unchanged if the cavity is axisymmetric. Before an illuminated cavity model can be declared a satisfactory match to the inner regions of Burnham's nebula, these problems need to be resolved by additional insights.

Another possibility is that the circumstellar and circumbinary disks thought to exist in the system could be related to the scattered light morphology. The circumstellar disk about T Tau N, detected but unresolved by the recent millimeter continuum observations (Akeson *et al.* 1998; Hogerheijde *et al.* 1997), is probably too small to be seen in our images. We would expect such a disk to be tidally truncated to an outer radius of order 0.3″, and thus would be completely hidden in our WFPC2 images by saturated pixels and instrumentally scattered light. A circumbinary disk would be significantly larger, perhaps comparable in scale to the nebular arc seen by HST. In the binary T Tauri star GG Tauri, where the binary separation is about half that of T Tau, a circumbinary disk of radius 400 AU is seen in scattered light with brightness between 10^{-3} and 10^{-4} of the stellar peak intensity

(Roddier *et al.* 1996). A ring of this size and brightness would just be detectable in our F555W image of T Tau; however, a larger and thus fainter ring would escape detection. The arc seen in the T Tau system does not appear similar to such a ring; however, a circumbinary ring can appear as an elliptical reflection nebulosity if it is viewed from near the disk plane. Another mechanism that could produce elliptical circumbinary structures is suggested by Lubow and Artymowicz 1996: an elliptical inner hole might be carved in a circumbinary disk by dynamical effects in a highly eccentric binary system.

Although we have not calculated models for the reflected light from eccentric circumbinary disks, we briefly consider the application of such models to T Tau. Any circumbinary disk is likely to be embedded within T Tau's extended, optically thick envelope (Calvet *et al.* 1994). Thus the circumbinary disk in this system, if it exists at all, could be hidden from direct illumination and consequently be unobservable in reflected light. Even absent this problem, there are significant difficulties in relating the observed nebulosity to a disk model. In this system the binary components appear projected on opposite sides of the nebular arc, rather than both being enclosed by it as seen in GG Tau. This could only be reconciled to the circumbinary disk models if the disk were viewed from near its equator plane, such that the scattering layer at the disk's upper surface would happen to be projected between the two stars (one of which would be highly extincted). A face-on disk with an elliptical hole is therefore excluded. The edge-on circumbinary disk model would also require a large elliptical inner hole to match the curvature and extent of the nebular arc; and the binary would have to be near periastron since both stars are displaced far from the center of the required arc/ellipse. This combination of special circumstances makes a disk model seem an unlikely explanation for the nebular arc, and thus some form of an illuminated ouflow cavity model seems the preferable one.

5. Conclusions

1. HST images reveal two extensions of reflection nebulosity within 2″ of T Tauri. They appear to form a single continuous nebular arc extending with some asymmetries from the N to the SW side of the optically visible star T Tau N.

2. The nebula morphology is generally similar to models of an illuminated outflow cavity opening toward the west-northwest and viewed from intermediate latitudes. The pole-on geometry previously assumed for the system is not consistent with the observations as modeled by an illuminated outflow cavity. Although our model can reproduce the general nebula geometry, it fails to account for the large limb brightening which is observed.

3. The infrared companion T Tau S was not directly detected at visual wavelengths, suggesting an extinction of at least 7 mag. We find no evidence of an optical tertiary component in the system.

6. Acknowledgements

NAS7-1260

This work is supported by NASA contract ~~NAS7-918~~ to the WFPC2 Investigation Definition Team at the Jet Propulsion Laboratory, California Institute of Technology. KRS also acknowledges support from the Origins of Solar Systems Research Program.

REFERENCES

Adams, F.C., Lada, C.J., and Shu, F.H. 1987, ApJ, 312, 788

Akeson, R. L., Koerner, D. W., and Jensen, E. L. N. 1998, ApJ, in press

Artymowicz, P., and Lubow, S.H. 1994, ApJ, 421, 651

Böhm, K.-H., and Solf, J. 1994, ApJ, 430, 277

Bührke, T., Brugel, E.W., and Mundt, R. 1986, A&A, 163, 83

Burrows, C.J. *et al.* 1996, ApJ, 473, 437

Burrows C. J. ed. "Hubble Space Telescope Wide Field and Planetary Camera 2 Instrument Handbook" Version 3.0, 1995, Space Telescope Science Institute, Baltimore.

Calvet, N., Hartmann, L., Kenyon, S. J., and Whitney, B. A. 1994, ApJ, 434, 330

Dyck, H. M., Simon, T., and Zuckerman, B. 1982, ApJ, 255, L103

Ghez, A. M., Neugebauer, G., Gorham, P. W., Haniff, C. A., Kulkarni, S. R., and Matthews, K. 1991, AJ, 102, 2066

Gilliland, R. L. 1994, ApJ, 435, L63

Gorham, P. W., Ghez, A. M., Haniff, C. A., Kulkarni, S. R., Matthews, K., and Neugebauer, G. 1992, AJ, 103, 953

Hogerheijde, M. R., van Langevelde, H. J., Mundy, L. G., Blake, G. A., and van Dishoeck, E. F. 1997, ApJ, 490, L99

Herbst, T. M., Robberto, M., and Beckwith, S.V.W. 1997, AJ, 114, 744

Herbst, T. M., Beckwith, S. V. W., Glindemann, A., Tacconi-Garman, L. E., Kroker, H., and Krabbe A. 1996, AJ, 111, 2403

Herbst, W., Booth, J. F., Chugainov, P.F., Zajtseva, G. V., Barksdale, W., Covino, E., Terranegra, L., Vittone, A., Verba, F. 1986, ApJ, 310, L71

Holtzman, J. A. *et al.* 1995, PASP, 107, 1065

Joy, A. H. 1945, ApJ, 102, 168

Kenyon, S., and Hartmann, L. 1995, ApJS, 101, 117

Krist, J.E., Burrows, C.J., Stapelfeldt, K.R. et al. 1997, ApJ, 481 447

Krist, J.E. 1995 in "Calibrating Hubble Space Telescope: Post Servicing Mission", STSci Baltimore p. 311

van Langevelde, H.J., van Dishoeck, E.F., van def Werf, P.P., and Blake G.A. 1994, A&A, 287, L25

Levreault, R.M. 1988, ApJS, 67, 283

Lubow, S.H., and Artymowicz, P. 1996, *Evolutionary Processes in Binary Stars*, R. Wijers, M. Davies, and C. Taut eds., Cambridge Univ. Press, p. 53 in press.

Maihara, T., and Kataza, H. 1991,A&A, 249, 392

Nakajima, T., and Golimowski, D. A. 1995, AJ, 109, 1181

Nisenson, P., Stachnik, R. V., Karovska, M., and Noyes, R. 1985, ApJ, 297, L17

Reipurth, B., Bally, J., and Devine, D. 1997, AJ, 114, 2708

Robberto, M., Clampin, M., Ligori, S., Paresce, F., Sacca, V., and Staude, H.J. 1995, A&A, 296, 431

Roddier, C., Roddier, F., Northcott, M.J., Graves, J.E., and Jim, K. 1996, ApJ, 463, 326

Schuster, K.-F., Harris, A. I., and Russell, A. P. G. 1997, A&A, 321, 568

Solf, J., Böhm, K.H., and Raga, A. 1988, ApJ, 334, 229

Strom, K. M., Strom, S. E., Edwards, S., Cabrit, S., and Skrutskie, M. F. 1989, AJ, 97, 1451

Ulrich, R.K. 1976, ApJ, 210,377

Whitney, B. A. and Hartmann, L. 1993, ApJ, 402, 605

This manuscript was prepared with the AAS LaTeX macros v4.0.

Fig. 1.— Greyscale WFPC2 images of T Tau showing the star and circumstellar nebulosity. The reduced PC1 F555W image is shown at top left. This same image is shown after subtraction of a scaled and aligned PSF in the top right panel. Similar PSF-subtraction results are obtained for the F675W and F814W images shown in the bottom two panels. In the difference images, saturated pixels in the images of T Tau and the PSF star result in bright and dark horizontal lines running through the stellar position. Position angle 35° points up on the figure; the field of view is 12″x10″.

Fig. 2.— Surface brightness map of the WFPC2 F555W image of T Tauri. An observed PSF was subtracted from the image. The dotted contour level is 15 mag arcsec^{-2} and contours are separated by 1 mag arcsec^{-2}. In this figure, north is up and east is to the left. Locations of the primary star and infrared companion are indicated by the two crosses. Offsets positions are with respect to the primary.

Fig. 3.— Axisymmetric cavity geometry used in the scattered light model. The observed impact parameter b between the star and the projected edge of the cavity constrains the shape parameters a,β for a specified observer latitude (see text).

Fig. 4.— Model reflection nebulae (panels a-c) for an axisymmetric cavity which reproduces the span, curvature and stellar impact parameter seen in the T Tau nebular arc. The model was calculated using a 3.5 AU internal grid and resampled to the Planetary Camera's resolution of 7 AU per pixel for T Tau. The HST F555W image is shown in panel d for comparison. Parameters of the nebula model are: panel a, $\theta = 25°, \beta = 3.6, a = 3\text{x}10^{-7}$; panel b, $\theta = 45°, \beta = 1.95, a = 5\text{x}10^{-3}$; and panel c, $\theta = 65°, \beta = 1.3, a = 0.33$.

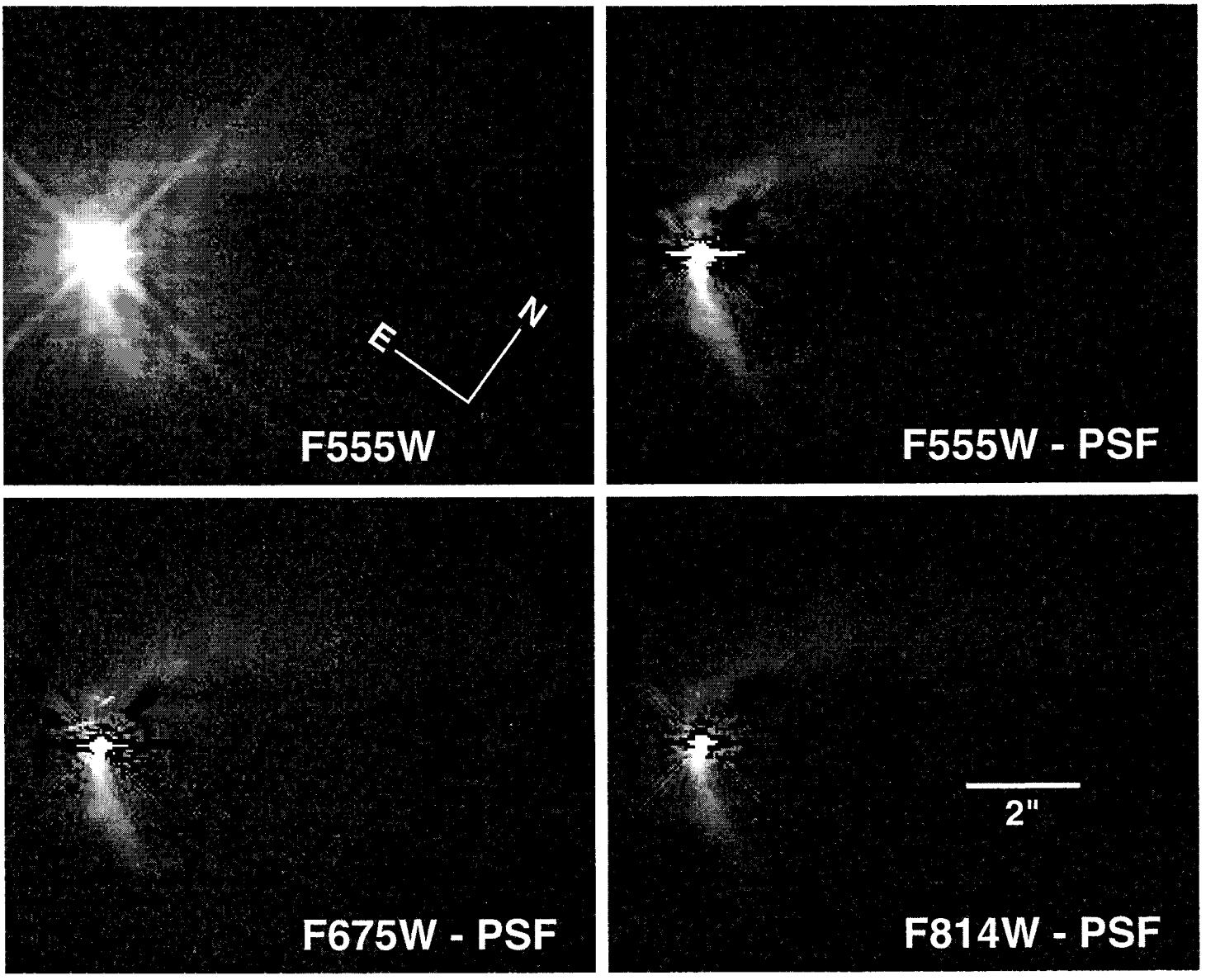
E
N
F555W
F555W - PSF
F675W - PSF
2"
F814W - PSF

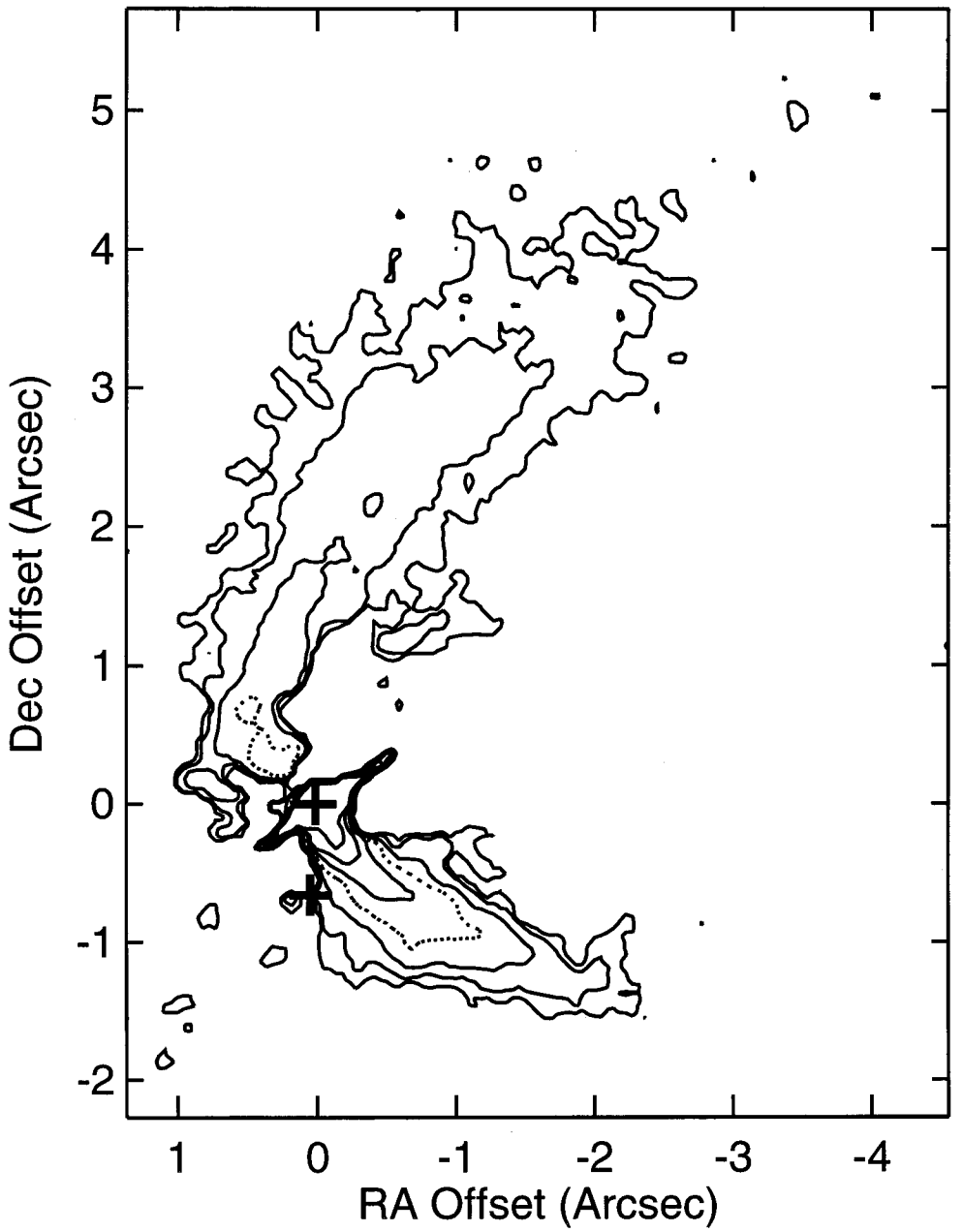
5
4
3
2
1
0
-1
-2
Dec Offset (Arcsec)
1
0
-1
-2
-3
-4
RA Offset (Arcsec)

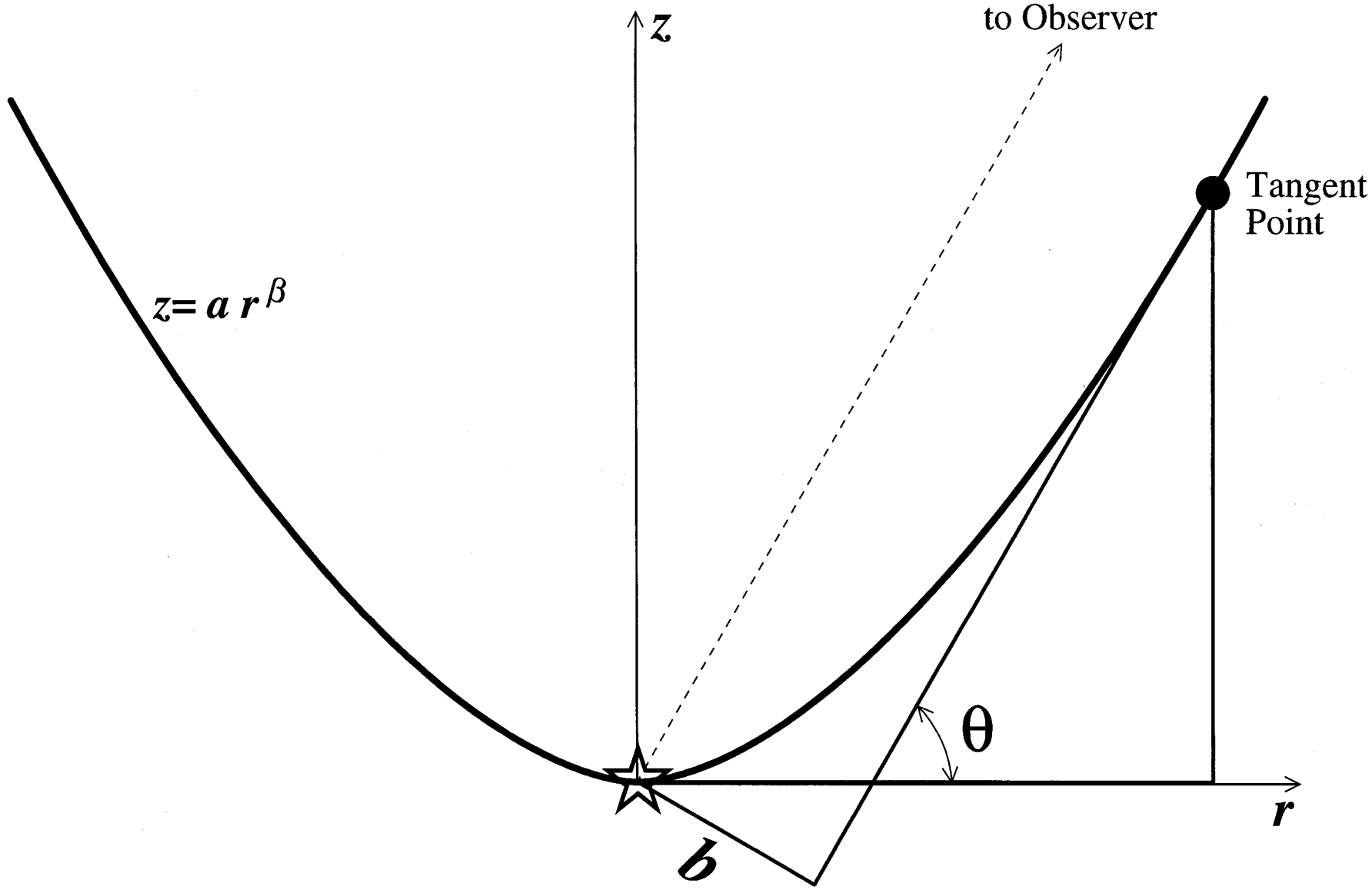
z
to Observer
Tangent
Point
$z = a\, r^{\beta}$
θ
r
b